Physics of Plasmas LETTER scitation.org/journal/php

A fluid simulation-based evidence of the soliton-type behavior of supersolitary waves in plasma

Cite as: Phys. Plasmas **26**, 100701 (2019); doi: 10.1063/1.5119993
Submitted: 15 July 2019 · Accepted: 12 September 2019 ·
Published Online: 2 October 2019

Ajay Lotekar,[a] Amar Kakad,[b] and Bharati Kakad[c]

AFFILIATIONS

Indian Institute of Geomagnetism, New Panvel (West), Navi Mumbai, India

[a]ablotekar@gmail.com
[b]amar@iigs.iigm.res.in
[c]ebharati@iigs.iigm.res.in

ABSTRACT

We performed a fluid simulation of the head-on collision of supersolitary waves (SSWs) with regular solitary waves (RSWs) in a plasma consisting of cold fluid ions and two-temperature electrons having kappa distributions. We have set up the fluid simulation to evolve both ion acoustic (IA) SSW and IA RSW self-consistently. Our simulation shows that the generated SSW and RSW maintain their shapes while propagating at a constant speed. Furthermore, the simulation demonstrates that the head-on collision of SSW with RSW does not affect their original characteristics, revealing their soliton-type behavior. This is the first simulation to confirm the soliton-type behavior of the SSWs in plasma.

Supersolitary waves (SSWs) are a new class of solitary waves,[1] which are characterized by having extra wiggles on both sides of their associated bipolar electric field structure.[2] Initially, SSWs were modeled in a complex plasma system that comprises four- or five-component plasma.[1] Later, Verheest *et al.*[3] reported that SSWs can be supported by a three-component plasma comprising positive and negative charged ions and nonthermal electrons. The existence of SSWs in different plasma systems has been investigated analytically by several authors.[3–12]

Kakad *et al.*[13] carried out the fluid simulation of ion acoustic (IA) SSWs in a plasma consisting of two-temperature kappa distributed electrons and cold fluid ions. They found that the Gaussian form of initial perturbations in the equilibrium electron and ion densities evolves into IA SSWs, which maintain the shape and the size during their propagation. However, whether such generated SSWs can survive after their collision with other solitary pulses was not addressed so far. Recently, Olivier *et al.*[14] have studied the overtaking collision properties of a small amplitude SSW with a RSW in a plasma consisting of cold ions and two-temperature Boltzmann electrons. Their study showed that the SSW alters its shape during the collision to form a RSW, implying that its collision with RSW is inelastic. Nevertheless, the results described in Fig. 2 in the study by Olivier *et al.*[14] show that the SSW loses its wiggles before encountering collision. In general, to confirm the soliton-type behavior of any wave pulses, the pulses should be stable before interacting with each other. However, the SSWs in their simulation seems to be unstable as its shape changes before its collision with the RSW.

In this paper, we perform the fluid simulation of the head-on collision of self-consistently generated stable SSW and RSW in plasma to examine the soliton type behavior of SSWs. In order to obtain SSW, Kakad *et al.*[13] used a large perturbation in the equilibrium densities of electrons and ions. However, the possibility of observing such a high magnitude perturbation in plasma is rare. We present here a new method which has successfully scaled down the order of perturbation required to excite the SSWs from much more realistic perturbations and investigated their collision with the RSW in plasma.

We consider a collisionless unmagnetized plasma consisting of cold fluid ion (H^+) and two electron (warm and hot) populations that follow kappa distributions.[13,15] The dynamics of ions are governed by the following continuity and momentum equations:

$$\frac{\partial N_i}{\partial t_n} + \frac{\partial (N_i U_i)}{\partial x_n} = 0, \tag{1}$$

$$\frac{\partial U_i}{\partial t_n} + U_i \frac{\partial U_i}{\partial x_n} = -\frac{\partial \Phi}{\partial x_n}, \tag{2}$$

where N_i and U_i are the normalized density and velocity of the ions in the x-direction, which are normalized as $N_i = n_i/n_{i0}$ and $U_i = v_i/C_{IA}$, respectively. Here, n_i and v_i are the unnormalized ion fluid density and velocity. n_{i0} is the equilibrium ion velocity. The characteristic IA sound speed $C_{IA} = (k_B T_{he}/m_i)^{1/2}$ is used in the velocity normalization, where T_{he} is the hot electron temperature and m_i is the mass of the ion. The space (x) and time (t) are normalized as $x_n = x/\lambda_{Dhe}$ and $t_n = \omega_{pi}t$. Here, $\lambda_{Dhe} = (k_B T_{he}\epsilon_0/n_{i0}e^2)^{1/2}$ is the hot electron Debye length and $\omega_{pi} = (n_{i0}e^2/\epsilon_0 m_i)^{1/2}$ is the ion plasma frequency.

The superthermal electrons in the system follow the kappa distribution.[15–20] The warm and hot electron densities are obtained by taking the first moment of their one-dimensional kappa velocity distribution function as

$$N_s = f_s\left[1 - \frac{\Phi}{\tau_s(\kappa_s - 3/2)}\right]^{-\kappa_s+1/2}, \tag{3}$$

where $s = we, he$ for warm and hot electrons, $f_s = n_{s0}/n_{i0}$, $\tau_s = T_s/T_{he}$. The densities of the warm (n_{we}) and hot (n_{he}) electrons are normalized as $N_{we} = n_{we}/n_{i0}$ and $N_{he} = n_{he}/n_{i0}$, respectively. The electrostatic potential (ϕ) is normalized as $\Phi = e\phi/k_B T_{he}$. κ_{we} and κ_{he} are the kappa indices associated with the warm and hot electrons, respectively. The electron and ion fluids are coupled by Poisson's equation,

$$\frac{\partial^2\Phi}{\partial x_n^2} = N_{we} + N_{he} - N_i. \tag{4}$$

In the fluid code, Eqs. (1), (2), and (4) are numerically solved in order to generate the SSW and RSW structures. We follow the same methodology in the fluid code as discussed by Kakad *et al.*[13] and Lotekar *et al.*[20–23] to solve Eqs. (1)–(4) numerically. The simulation parameters used in this study are a grid spacing of $\triangle x = 0.2\ \lambda_{Dhe}$, a time interval of $\Delta t = 0.1\ \omega_{pi}^{-1}$, and a system length of $L_x = 30000\lambda_{Dhe}$. To evolve the SSW and RSW in the simulation, we introduce the perturbations in the equilibrium electron and ion densities by using the following equation:

$$n_s(x) = n_{s0} + \Delta n_s\ \exp\left[-\left(\frac{x - x_0}{l_{0ns}}\right)^2\right]. \tag{5}$$

Along with the density perturbations, we have simultaneously used the velocity perturbation in the equilibrium velocity of the ions by using the following equation:

$$v_i(x) = v_{i0} + \Delta v_i\ \exp\left[-\left(\frac{x - x_0}{l_{0vi}}\right)^2\right]. \tag{6}$$

The simultaneous injection of density and velocity perturbations in the ion fluid is analogous to the injection of the ions with a certain velocity in the plasma. In Eqs. (5) and (6), Δn_s and l_{0ns} are the amplitude and the width of the density perturbation, respectively, whereas Δv_i and l_{0vi} are the amplitude and the width of velocity perturbation, respectively. x_0 is the position of perturbation placed in the simulation system. The parameters considered in the simulation are $f_{we} = 0.055$, $f_{he} = 1 - f_{we}$, $\tau_{we} = 0.12$, $\tau_{he} = 1$, $\kappa_{ce} = 10$, and $\kappa_{he} = 10$. The ion flow velocity (v_{i0}) at $t = 0$ is assumed to be zero. We have injected two different sets of density and velocity perturbations in the system at two different places and timings in such a way that one set of perturbations self-consistently evolves into the stable SSW and the other into RSW. We have allowed them to interact with each other by considering the periodic boundary conditions in the simulation.[24] The perturbation parameters, their time of injection, and places for two different sets of perturbations for the excitation of SSW and RSW in the simulation are given in Table I.

Figure 1 shows snapshots of the evolution of the electric field associated with the SSW (top panels) and RSW (bottom panels) at different timings through such perturbations. First, we discuss the evolution of SSW. At $\omega_{pi}t = 0$, we have injected the perturbations in the equilibrium densities of the electrons and ions and also in the equilibrium ion velocity at the position $x_0 = 0$ in the system, which generate the bipolar electric field pulse in the system as shown in Fig. 1(a). It is seen that this bipolar pulse does not split into two identical pulses as reported in an earlier study by Kakad *et al.*[13] (see Fig. 1 in the study by Kakad *et al.*[13]), which is due to the injection of velocity perturbation along with the density perturbations in the present case. In this scenario, a significant amount of ion fluid from the localized perturbed density area comes under the influence of the velocity perturbation. The positive velocity perturbation accelerates this ion fluid from the localized perturbed region along the rightward direction, leaving some of the ion fluid behind that do not come under the influence of the velocity perturbation. This process systematically set up two localized charge separation regions with distinct characteristics, which subsequently develop two distinguishable oppositely propagating localized electric field pulses as shown in Fig. 1(b). It is observed that the rightward propagating large amplitude pulse evolved into the SSW pulse, while the leftward propagating small amplitude pulse evolved into the IA oscillations (see supplementary material-I). We have shown here only the evolution of the rightward propagating bipolar pulse. In the evolution of this bipolar pulse, second local extrema ("wiggles") with different amplitudes are formed on each side of the pulse [see Fig. 1(c)]. Later, these extrema achieve comparable amplitudes by releasing the oscillations from the trailing side of the pulse. This gives the symmetric shape to the pulse alike SSW as shown in Fig. 1(d). We confirm this pulse as a stable SSW as it propagates with the constant speed in a space without changing its shape and size.

To generate the RSW, we have injected another set of localized density and velocity perturbations in the equilibrium ion and electron densities and ion fluid velocity at $\omega_{pi}t = 1070$. In this case, the amplitudes and widths of the perturbations are smaller as compared to the earlier set of perturbations (see Table I). To evolve a stable RSW pulse,

TABLE I. The perturbation parameters used for the generation of SSW and RSW in the simulation.

Perturbation		SSW	RSW	Normalizing unit
Density (s=we, he, i)	Δn_s	0.32	0.2	n_{0i}
	l_{n0s}	31	10	λ_{Dhe}
Velocity (s=i)	Δv_s	0.4	−0.1	C_{IA}
	l_{v0s}	20	20	λ_{Dhe}
Position	x_0	0	−12875	λ_{Dhe}
Time	t	0	1070	ω_{pi}^{-1}

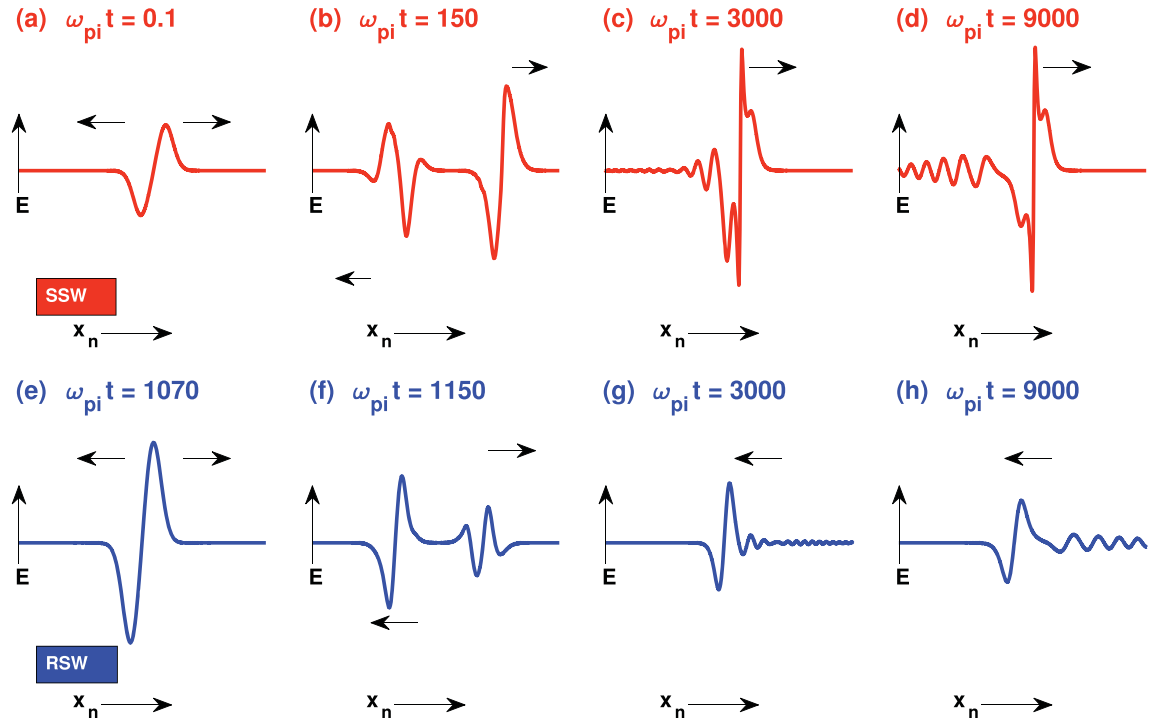

FIG. 1. Snapshots of the electric field pulses in the course of evolution of SSW (top panel) and RSW (bottom panel). In panels (c), (d), (g), and (h), we have shown only the leftward propagating pulse in the simulation.

these perturbations are injected at the location ($x_0 = -12875\lambda_{Dhe}$) which is far away from the waves and oscillations evolved through the first set of perturbations. This injected perturbations result in a bipolar pulse at $\omega_{pi}t = 1070$ [as shown in Fig. 1(e)], which later evolves into two distinguishable oppositely propagating pulses as shown in Fig. 1(f). The generation mechanism of these pulses is similar to the earlier case except for their directions of propagation, which is due to the negative velocity perturbation. Further, the leftward propagating pulse evolves into the asymmetric bipolar IA solitary wave pulse as depicted in Fig. 1(g), whereas the rightward propagating pulse evolved as IA oscillations (see the supplementary material). Later, this asymmetric IA pulse evolved as a stable symmetric bipolar RSW pulse. One of its snapshots at $\omega_{pi}t = 9000$ is shown in Fig. 1(h). We have used the negative velocity perturbation here so that an evolved RSW after reaching the left-side boundary enters the right-side boundary due to the periodic boundaries considered in the simulation. In this way, the head-on collision of the RSW and SSW will occur, which is shown in Fig. 2(a). Figure 2(a) shows the spatiotemporal evolution of electrostatic potential in the system in which the evolution of SSW, RSW, and IA oscillations is evident through different color bands. In the simulation, we have made sure that the SSW and RSW should get enough space and time to evolve themselves as stable structures before their collision. Figure 2(a) shows the constant slopes of both SSW and RSW bands after their formation at $\omega_{pi}t = 9000$ up to the time of their collision, which confirms the propagation of SSW and RSW pulses with the constant speeds. During this time, the amplitudes of SSW and RSW remain constant. This shows that the SSW and RSW structures first acquire stability while approaching each other, and then, their head-on collision occurs at $\omega_{pi}t = 11220$. The space-time region around their head-on collision is marked with the rectangle in Fig. 2(a), which is zoomed in Fig. 2(b). During the collision, both pulses merge with each other and then get separated. One of the snapshots of the electric field profile associated with collision of the SSW with RSW at $\omega_{pi}t = 11200$ is shown in Fig. 2(c). The collision of the oscillations with the RSW and SSW pulses also makes their shape little distorted. However, as the RSW and SSW pulses come out from the oscillations, the pulses acquire their original shapes. To examine the change in their shapes after collision, we have plotted their associated electric field profiles at before and after the collision time, which is shown in Fig. 3. In this figure, we have plotted the SSW and RSW pulses at their respective positions for two-time instances in such a way that we can easily compare their shapes before and after the collision. To do so, we have used two different x-axes to show the exact spatial extent of these pulses in the simulation at different timings. The bottom x-axis (blue color) shows the positions of the pulses before the collision time ($\omega_{pi}t = 10490$), and the top x-axis (red color) shows the positions of the pulses after the collision time ($\omega_{pi}t = 12990$). This figure illustrates that the shapes of SSW and RSW structures before (blue profiles) and after (red profiles) collision are unchanged. This demonstrates that the collision between the SSW and RSW is elastic in nature. In addition to this, we have also tracked the variations in the maximum amplitudes of both the RSW and SSW before and after the collision (see the supplementary material), which confirms that there is no change in the amplitudes of SSW and RSW before and after the collision. To get

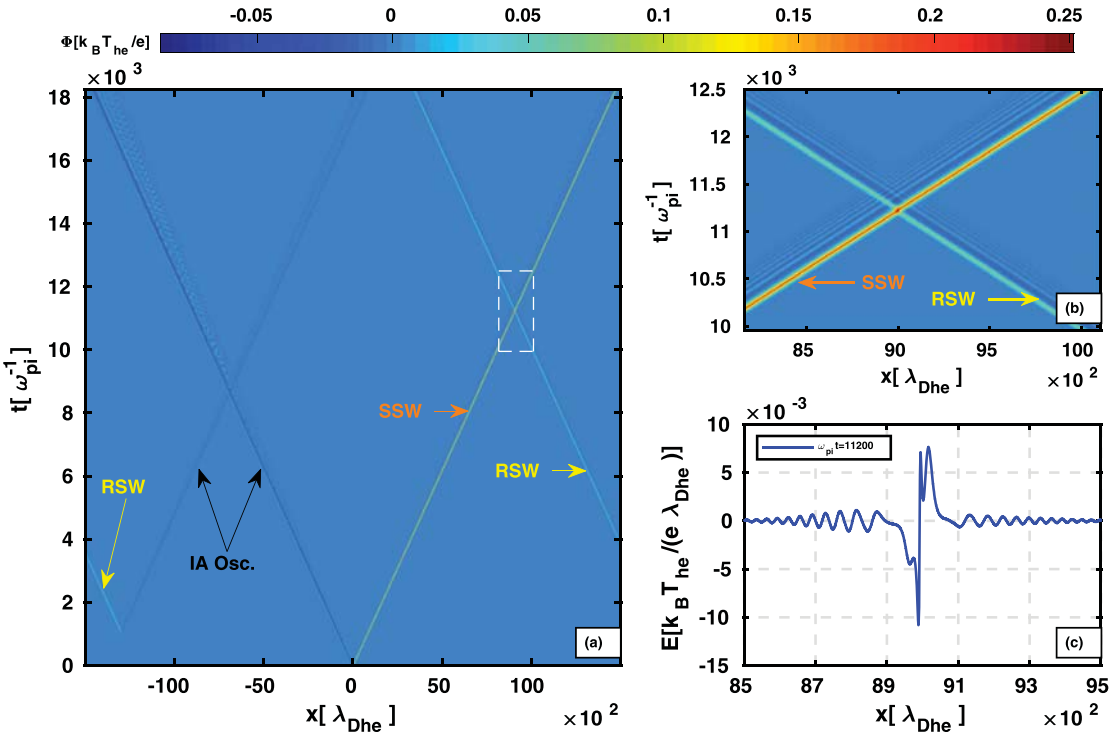

FIG. 2. (a) Spatiotemporal variation of potential (ϕ) in the simulation. Different color bands show the potential associated with the SSW, RSW, and IA oscillations. The region marked by the rectangle shows the region in which the head-on collision of SSW and RSW takes place. This region is zoomed in panel (b). One of the snapshots of the electric field structures associated with the SSW and RSW during their collision at $\omega_{pi}t = 11200$ is depicted in panel (c).

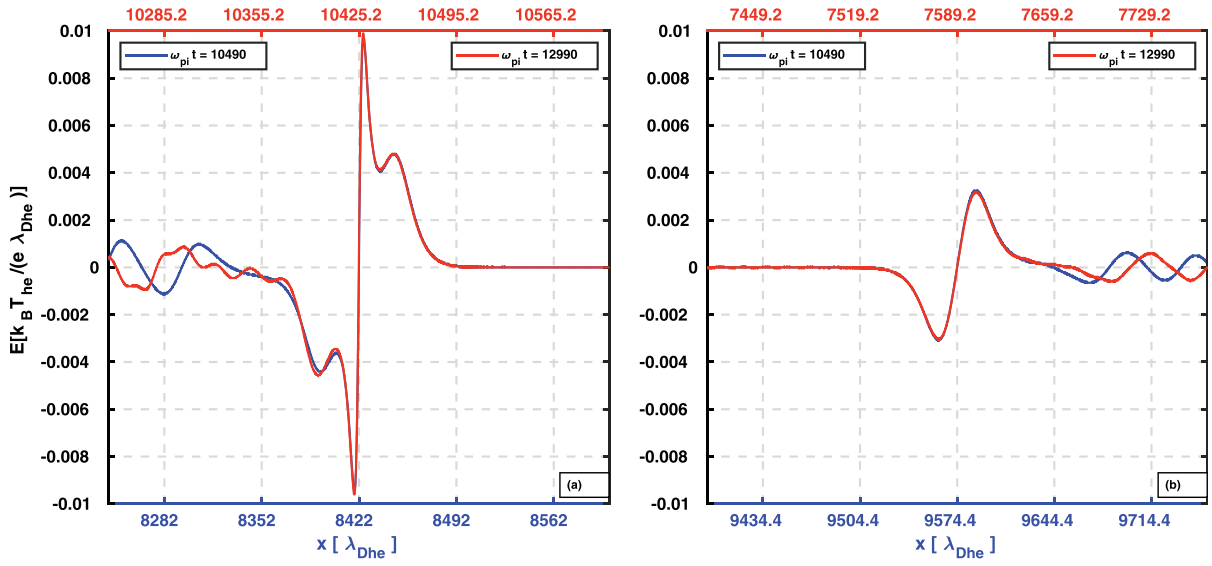

FIG. 3. The profiles of the (a) SSW and (b) RSW before (at $\omega_{pi}t = 10490$) and after collision (at $\omega_{pi}t = 12990$) times. The profiles before the collision are shown in blue color, whereas the profiles after the collision are shown in red color. The bottom *x*-axis (blue color) is associated with the pulses before the collision time, and the top *x*-axis (red color) is associated with the pulses after the collision time.

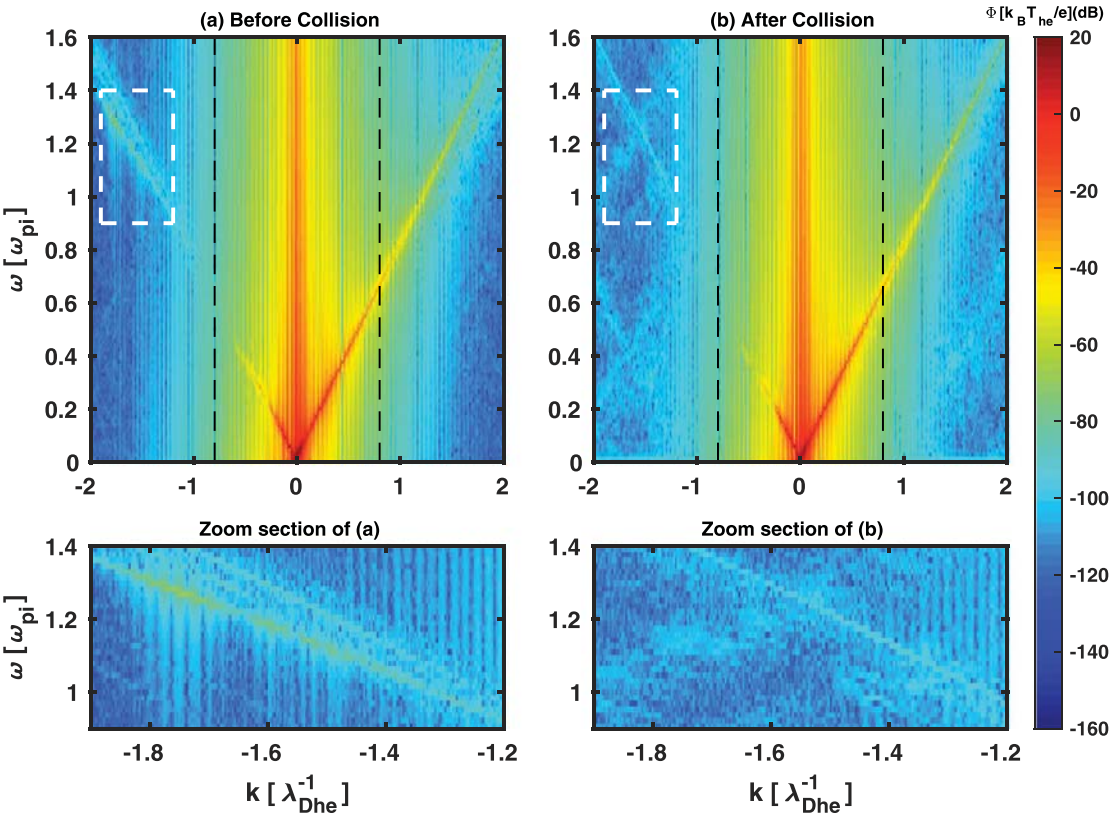

FIG. 4. The FFT of the potential in the simulation for the time spans (a) $\omega_{pi}t = 9400$–9700 (before collision) and (b) $\omega_{pi}t = 14500$–14800 (after collision). The bottom panels are the zoomed section marked by the rectangle in panels (a) and (b).

more physical insight into the collision process between the RSW and SSW, a two-dimensional fast Fourier transform (FFT) of the potential (Φ) in the system is shown in Fig. 4 for the time spans $\omega_{pi}t = 9400$–9700 (before collision) and $\omega_{pi}t = 14500$–14800 (after collision). The bottom panels in this figure show the zoomed portion of the regions marked with the rectangles in panels (a) and (b). In the system, the SSW propagates in the rightward direction throughout the simulation time and the RSW propagates in the leftward direction. Hence, in Fig. 4, the dispersion curve on the positive x-axis is associated with the SSW, whereas the dispersion on the negative x-axis is associated with the RSW. In Fig. 4(a), it can be seen that the energy given to the system in the excitation of SSW is distributed among the wide range of wavelengths. In the excitation of RSW, the strength of the perturbation is weak as compared to the perturbation used to excite the SSW. Hence, most of its power is limited to the long wavelength modes.[20,21,25] In this case, a weak dispersion associated with the short wavelength modes is also visible in the white rectangle area which is zoomed in the bottom panel in Fig. 4(a). These short wavelength modes are due to the IA oscillations which are found to be dispersive in nature. In panels (a) and (b) of Fig. 4, we do not observe any change in the dispersions of the SSW and RSW before and after collision as they are nondispersive in nature. This indicates that both RSW and SSW maintain their shapes while propagating in the system with the constant phase speeds before and after the collision. This again confirms that the collision of SSW and RSW is elastic. Furthermore, it is observed that the short wavelength region (the region marked with white rectangles) manifested the interesting fact that some of the short wavelength modes which have significant power before the collision have weakened after the collision. This is because the short wavelength modes are dispersive in nature.[20,21,25,26]

In general, a solitary wave pulse in plasma is termed as a soliton when it satisfies the following conditions: (1) it must maintain its shape when it moves at a constant speed and (2) when a soliton interacts with another soliton, it emerges from the "collision" unchanged. Our simulation shows that the supersolitary wave pulse generated in the system maintains its shape when it moves with constant speed. Furthermore, the simulation shows that the supersolitary pulse emerges unchanged after its interaction with the regular soliton. Hence, to conclude, this letter reveals the soliton type behavior of the SSW and proposes that the supersolitary wave can be termed as a "supersoliton."

See the supplementary material for the animation of the head-on collision of self-consistently evolved SSW and RSW (bottom panel), which is created from the simulation data. The moving red color window in the animation tracks the pulse which evolves into SSW, a

zoomed version of which is shown in the first upper panel. Another magenta color window tracks the pulse which evolves into RSW. A zoomed version of it is shown in the second upper panel. Supplementary material (II) shows maximum potentials (Φ_{max}) of the RSW (blue curve) and SSW (red curve) in the simulation.

The model computations were performed on the High Performance Computing System at the Indian Institute of Geomagnetism.

REFERENCES

[1]A. Dubinov and D. Y. Kolotkov, Plasma Phys. Rep. **38**, 909 (2012).
[2]A. E. Dubinov and D. Y. Kolotkov, Rev. Mod. Plasma Phys. **2**, 2 (2018).
[3]F. Verheest, M. A. Hellberg, and I. Kourakis, Phys. Plasmas **20**, 012302 (2013).
[4]M. A. Hellberg, T. K. Baluku, F. Verheest, and I. Kourakis, J. Plasma Phys. **79**, 1039 (2013).
[5]S. Singh and G. Lakhina, Commun. Nonlinear Sci. Numer. Simul. **23**, 274 (2015).
[6]C. Olivier, S. Maharaj, and R. Bharuthram, Phys. Plasmas **22**, 082312 (2015).
[7]S. V. Steffy and S. S. Ghosh, Phys. Plasmas **24**, 102111 (2017).
[8]D.-N. Gao, J. Zhang, Y. Yang, and W.-S. Duan, Plasma Phys. Rep. **43**, 833 (2017).
[9]S. S. Varghese and S. S. Ghosh, Phys. Plasmas **23**, 082304 (2016).
[10]C. P. Olivier, F. Verheest, and S. K. Maharaj, J. Plasma Phys. **83**(6), 905830605 (2017).
[11]S. V. Steffy and S. S. Ghosh, Phys. Plasmas **25**, 062302 (2018).
[12]A. Paul and A. Bandyopadhyay, Indian J. Phys. **92**, 1187 (2018).
[13]A. Kakad, A. Lotekar, and B. Kakad, Phys. Plasmas **23**, 110702 (2016).
[14]C. P. Olivier, F. Verheest, and W. A. Hereman, Phys. Plasmas **25**, 032309 (2018).
[15]F. Verheest, M. A. Hellberg, and I. Kourakis, Phys. Plasmas **20**, 082309 (2013).
[16]M. Hellberg, R. Mace, T. Baluku, I. Kourakis, and N. Saini, Phys. Plasmas **16**, 094701 (2009).
[17]I. Kourakis, S. Sultana, and M. Hellberg, Plasma Phys. Controlled Fusion **54**, 124001 (2012).
[18]G. Livadiotis and D. McComas, Space Sci. Rev. **175**, 183 (2013).
[19]G. Livadiotis, J. Geophys. Res.: Space Phys. **120**, 1607, https://doi.org/10.1002/2014JA020825 (2015). 2014JA020825.
[20]A. Lotekar, A. Kakad, and B. Kakad, Phys. Plasmas **23**, 102108 (2016).
[21]A. Lotekar, A. Kakad, and B. Kakad, Phys. Plasmas **24**, 102127 (2017).
[22]A. Lotekar, A. Kakad, and B. Kakad, Commun. Nonlinear Sci. Numer. Simul. **68**, 125 (2019).
[23]A. Lotekar, A. Kakad, and B. Kakad, J. Geophys. Res.: Space Phys. **124** (2019).
[24]A. Kakad, B. Kakad, and Y. Omura, Phys. Plasmas **24**, 060704 (2017).
[25]A. Kakad, Y. Omura, and B. Kakad, Phys. Plasmas **20**, 062103 (2013).
[26]A. Kakad and B. Kakad, Phys. Plasmas **23**, 122101 (2016).